




The Neutrally Charged Diarylurea Compound PQ401 Kills Antibiotic-Resistant and Antibiotic-Tolerant *Staphylococcus aureus*

Wooseong Kim,^a Guijin Zou,^b Wen Pan,^c Nico Fricke,^d Hammad A. Faizi,^e Soo Min Kim,^a Rajamohammed Khader,^c Silei Li,^c Kiho Lee,^c Iliana Escorba,^c Petia M. Vlahovska,^f Huajian Gao,^{b,g} Frederick M. Ausubel,^{h,i}  Eleftherios Mylonakis^c

^aCollege of Pharmacy, Graduate School of Pharmaceutical Sciences, Ewha Womans University, Seoul, Republic of Korea

^bInstitute of High Performance Computing, A*STAR, Singapore, Singapore

^cDivision of Infectious Diseases, Rhode Island Hospital, Warren Alpert Medical School of Brown University, Providence, Rhode Island, USA

^dDepartment of Molecular Physiology and Biological Physics, University of Virginia School of Medicine, Charlottesville, Virginia, USA

^eDepartment of Mechanical Engineering, Northwestern University, Evanston, Illinois, USA

^fDepartment of Engineering Sciences and Applied Mathematics, Northwestern University, Evanston, Illinois, USA

^gSchool of Mechanical and Aerospace Engineering, College of Engineering, Nanyang Technological University, Singapore, Singapore

^hDepartment of Molecular Biology, Massachusetts General Hospital, Boston, Massachusetts, USA

ⁱDepartment of Genetics, Harvard Medical School, Boston, Massachusetts, USA

ABSTRACT Resistance or tolerance to traditional antibiotics is a challenging issue in antimicrobial chemotherapy. Moreover, traditional bactericidal antibiotics kill only actively growing bacterial cells, whereas nongrowing metabolically inactive cells are tolerant to and therefore “persist” in the presence of legacy antibiotics. Here, we report that the diarylurea derivative PQ401, previously characterized as an inhibitor of the insulin-like growth factor I receptor, kills both antibiotic-resistant and nongrowing antibiotic-tolerant methicillin-resistant *Staphylococcus aureus* (MRSA) by lipid bilayer disruption. PQ401 showed several beneficial properties as an antimicrobial lead compound, including rapid killing kinetics, low probability for resistance development, high selectivity to bacterial membranes compared to mammalian membranes, and synergism with gentamicin. In contrast to well-studied membrane-disrupting cationic antimicrobial low-molecular-weight compounds and peptides, molecular dynamic simulations supported by efficacy data demonstrate that the neutral form of PQ401 penetrates and subsequently embeds into bacterial lipid bilayers more effectively than the cationic form. Lastly, PQ401 showed efficacy in both the *Caenorhabditis elegans* and *Galleria mellonella* models of MRSA infection. These data suggest that PQ401 may be a lead candidate for repurposing as a membrane-active antimicrobial and has potential for further development as a human antibacterial therapeutic for difficult-to-treat infections caused by both drug-resistant and -tolerant *S. aureus*.

IMPORTANCE Membrane-damaging antimicrobial agents have great potential to treat multidrug-resistant or multidrug-tolerant bacteria against which conventional antibiotics are not effective. However, their therapeutic applications are often hampered due to their low selectivity to bacterial over mammalian membranes or their potential for cross-resistance to a broad spectrum of cationic membrane-active antimicrobial agents. We discovered that the diarylurea derivative compound PQ401 has antimicrobial potency against multidrug-resistant and multidrug-tolerant *Staphylococcus aureus*. PQ401 selectively disrupts bacterial membrane lipid bilayers in comparison to mammalian membranes. Unlike cationic membrane-active antimicrobials, the neutral form of PQ401 rather than its cationic form exhibits maximum membrane activity. Overall, our results demonstrate that PQ401 could be a promising

Citation Kim W, Zou G, Pan W, Fricke N, Faizi HA, Kim SM, Khader R, Li S, Lee K, Escorba I, Vlahovska PM, Gao H, Ausubel FM, Mylonakis E. 2020. The neutrally charged diarylurea compound PQ401 kills antibiotic-resistant and antibiotic-tolerant *Staphylococcus aureus*. mBio 11:e01140-20. <https://doi.org/10.1128/mBio.01140-20>.

Editor Martin J. Blaser, Rutgers University

Copyright © 2020 Kim et al. This is an open-access article distributed under the terms of the [Creative Commons Attribution 4.0 International license](https://creativecommons.org/licenses/by/4.0/).

Address correspondence to Eleftherios Mylonakis, emylonakis@lifespan.org.

This article is a direct contribution from Eleftherios Mylonakis, a Fellow of the American Academy of Microbiology, who arranged for and secured reviews by Alejandro Aballay, School of Medicine, Oregon Health & Science University; Tongtao Yue, China University of Petroleum; and Sulin Zhang, The Pennsylvania State University.

Received 5 May 2020

Accepted 21 May 2020

Published 30 June 2020

lead compound that overcomes the current limitations of membrane selectivity and cross-resistance. Also, this work provides deeper insight into the design and development of new noncharged membrane-targeting therapeutics to combat hard-to-cure bacterial infections.

KEYWORDS persists, antibiotic tolerance, antimicrobial resistance, MRSA, membrane-active antimicrobials, antibiotic, bacterial persister, *Caenorhabditis elegans*, membrane-active agent

Staphylococcus aureus is a Gram-positive bacterial pathogen that colonizes the skin or nasal cavity of approximately one-third of the human population (1). *S. aureus* is one of the most significant human bacterial pathogens, causing a wide range of infections from mild skin infections and food poisoning to life-threatening infections, such as toxic shock syndrome, endocarditis, and osteomyelitis (1). Despite advances in antibiotic chemotherapy, including the introduction of daptomycin in 2003, treatment of *S. aureus* infections is still a challenge due to resistance to or tolerance of clinically used antibiotics, as exemplified by methicillin-resistant *S. aureus* (MRSA) or vancomycin-intermediate or -resistant *S. aureus* (VISA/VRSA).

S. aureus can readily acquire resistance by horizontal gene transfer (2). Without acquiring genetic mutations that actively confer antibiotic resistance, nongrowing metabolically inactive *S. aureus* cells also exhibit high levels of tolerance to currently used antibiotics (3–7). In a laboratory setting, the proportion of antibiotic-tolerant cells in an *S. aureus* population varies depending on growth phase (5, 8). In stationary phase, essentially the entire bacterial population will survive prolonged treatment with high concentrations of bactericidal antibiotics (3, 4, 6, 8). This has recently been defined as antibiotic “tolerance” (9). In contrast, in lag and early exponential phase, only a small subpopulation of an *S. aureus* culture will survive antibiotic treatment (8). In this case, the survivors are designated “persisters” (9).

Antibiotic tolerance is a consequence of the fact that traditional antibiotics target biosynthetic processes that are occurring at significantly reduced levels in nongrowing cells (10) or is a consequence of a low-energy state that arrests the energy-dependent uptake of antibiotics (5, 7). Clinically, bacterial tolerance or persistence is associated with the recalcitrance of chronic infections (11, 12). The present lack of effective antibiotics against antibiotic-resistant bacteria or tolerant/persister cells highlights the unmet need of developing novel antimicrobial therapies.

The validity of the bacterial membrane as an antimicrobial target has been proven by the evolution of antimicrobial peptides (AMPs) and proteins by animals, plants, and fungi that kill bacteria by disrupting bacterial membranes (13). Bacterial membranes are an ideal target for antimicrobial agents because membrane integrity is indispensable for bacterial survival regardless of growth state (14). However, a key barrier to the development of membrane-active agents as human therapeutics is their typical low level of selectivity between bacterial and mammalian membranes. Since natural AMPs exhibit high selectivity to bacterial over mammalian membranes, membrane-active small molecules are typically designed and developed to mimic natural AMPs (15, 16). Thus, rationally designed membrane-active small molecules are usually cationic and amphipathic, which are key structural features of AMPs (15, 16). In particular, the cationic nature of natural AMPs plays an important role in selectively binding to negatively charged bacterial membranes by electrostatic affinity rather than binding to zwitterionic mammalian membranes (15, 17, 18). However, bacteria can acquire resistance to cationic membrane-active agents by reducing the negative charge of their membranes, which can subsequently result in cross-resistance to a range of natural AMPs, including host innate immunity effectors and other synthetic cationic membrane-active antimicrobials (17, 18). Therefore, development of membrane-active small molecules that show high levels of bacterial membrane selectivity while at the same time minimizing the selection of cross-resistance remains challenging.

Recently, our group used a SYTOX Green-MRSA membrane permeability assay (19)

to screen a collection of 185 “hits” obtained by screening ~82,000 synthetic chemicals using an automated high-throughput *Caenorhabditis elegans*-MRSA intestinal infection assay (20). This strategy enables us to exclude toxic compounds with low membrane selectivity because the hit is determined based on *C. elegans* survival. Using this approach, we were able to identify a set of membrane-active antimicrobials effective against nongrowing MRSA. These membrane-disrupting compounds exhibited high levels of membrane selectivity to bacterial compared to mammalian membranes (6, 20, 21).

Diarylureas are known to be important pharmacophores in drug discovery (22). Indeed, diarylurea derivatives have been developed as antimalarial (23), antischistosomal (24), antimicrobial (25, 26), and anticancer (22, 27) agents. We identified the diarylurea compound PQ401 as a hit in the *C. elegans* screen (described above) that not only blocks the ability of MRSA to kill *C. elegans* but also induces rapid MRSA membrane permeabilization. PQ401 has been shown to inhibit autophosphorylation of the insulin-like growth factor I receptor (IGF-1R) and impede breast cancer cell growth in *in vivo* mouse models (28). However, the antimicrobial activity of PQ401 has not been previously reported. In this paper, we elucidate the mode of action by which PQ401 permeabilizes the membrane and the role that ionized states of PQ401 play in its antimicrobial potency. Unexpectedly, we found that the neutral form of PQ401 is more potent than the cationic form, which correlates with enhanced membrane penetration of the neutral form in molecular dynamics simulation studies. In addition, we report that PQ401 has promising features as a potential therapeutic including high potency against both multidrug-resistant and multidrug-tolerant Gram-positive pathogens, fast killing kinetics, a very low rate of resistance development, and synergism with gentamicin.

RESULTS

PQ401 exhibits bactericidal activity and a low probability for resistance development. We identified PQ401 (Fig. 1A) as a hit compound that rescues *C. elegans* from MRSA-mediated killing (Fig. 1B) (20). In general, a compound can rescue *C. elegans* from an MRSA intestinal infection if it inhibits bacterial growth, blocks a bacterial virulence factor or factors, or modulates *C. elegans* innate immunity (29–31). We first tested the antimicrobial activity of PQ401 against a panel of antibiotic-resistant *S. aureus* strains, including MRSA clinical isolates and a vancomycin-resistant *S. aureus* (VRSA; strain VRS1) (32). As shown in Table 1, the MIC of PQ401 was 4 $\mu\text{g/ml}$ against all of the MRSA strains tested as well as the VRSA strain VRS1 (Table 1). PQ401 demonstrated bactericidal activity with a minimum bactericidal concentration (MBC) of 4 $\mu\text{g/ml}$ against a panel of MRSA and VRSA strains (Table 2). It exhibited fast killing kinetics, completely eradicating 5×10^7 CFU/ml of growing MRSA at 10 $\mu\text{g/ml}$ within 4 h, indicating that PQ401 is a more effective bactericidal agent than vancomycin against MRSA (Fig. 1C).

We further tested the antimicrobial activity of PQ401 using a panel of the so-called ESKAPE pathogens, which include two Gram-positive bacteria (*Enterococcus faecium* and *S. aureus*) and four Gram-negative bacteria (*Klebsiella pneumoniae*, *Acinetobacter baumannii*, *Pseudomonas aeruginosa*, and *Enterobacter* spp.). These ESKAPE pathogens are of particular concern because they are the leading cause of nosocomial infections and often develop antibiotic resistance (33). PQ401 showed antimicrobial activity against Gram-positive pathogens but not against Gram-negative pathogens (Table 3). Interestingly, PQ401 has an MIC of 4 $\mu\text{g/ml}$ against the multidrug-resistant *E. faecium* strain C68 (34) (Table 3) as it does against the *S. aureus* strains tested.

S. aureus can readily develop resistance against most clinical antibacterial agents (35). To evaluate the ability of *S. aureus* to develop resistance to PQ401, we exposed three independent cultures of MRSA strain MW2 (SP1, SP2, and SP3) to a sub-MIC level of PQ401 for 25 days using a serial passage method in a 96-well plate (36). The fluoroquinolone antibiotic ciprofloxacin targeting DNA gyrase was used as a control. MRSA MW2 strains exhibiting a 32-fold-higher MIC to ciprofloxacin than the wild-type strain were generated after 25 days of serial passage in sub-MICs (Fig. 1D). In contrast,

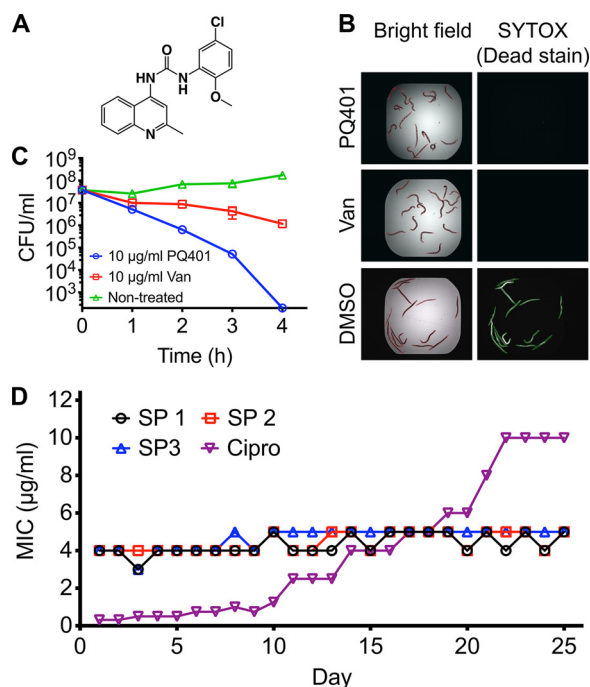


FIG 1 The insulin-like growth factor receptor (IGF-1R) inhibitor PQ401 exhibits bactericidal activity against *S. aureus* strain MW2 with no detectable resistance development. (A) Chemical structure of PQ401. (B) MRSA-infected *C. elegans* was treated with 5 µg/ml PQ401, 10 µg/ml vancomycin (Van, positive control), and 0.1% DMSO (DMSO, negative control). Dead worms were stained with SYTOX Orange. (C) Exponential-phase *S. aureus* MW2 was treated with PQ401 or vancomycin for 4 h. The bacterial viability was measured at hourly intervals. The limitation of detection is 2×10^2 CFU/ml. Error bars denote SD ($n = 3$). (D) Three attempts to develop MRSA resistance to PQ401 (SP 1, 2, and 3) and to ciprofloxacin (Cipro) over 25 days.

we did not observe a significant increase in the PQ401 MIC during the same time frame (Fig. 1D). This result suggests that PQ401 exhibits an extremely low probability for PQ401 resistance development.

PQ401 selectively disrupts bacterial membranes. The finding that PQ401 exhibits a high rate of killing and a low probability of resistance development suggests that it might be functioning as a membrane-active antimicrobial (14, 37). To test whether PQ401 disrupts MRSA membranes, we measured the permeability of MRSA MW2 to SYTOX Green after treatment with a range of concentrations of PQ401. As shown in Fig. 2A, PQ401 induced rapid membrane permeabilization in a dose-dependent manner. Dose-dependent permeabilization was also observed in nongrowing antibiotic-

TABLE 1 MIC of PQ401 against MRSA strains

MRSA strain	MIC (µg/ml) of drug:		
	Oxacillin	Vancomycin	PQ401
MW2	64	1	4
ATCC 33591	>64	2	4
JE2	64	1	4
VRS1	>64	>64	4
BF1	>64	2	4
BF2	>64	2	4
BF3	32	2	4
BF4	16	2	4
BF5	>64	1	4
BF7	>64	2	4
BF8	>64	2	4
BF10	>64	1	4
BF11	>64	1	4

TABLE 2 Minimum bactericidal concentration of PQ401 against MRSA strains

MRSA strain	MBC ($\mu\text{g/ml}$) of drug:		
	Oxacillin	Vancomycin	PQ401
MW2	>64	4	4
ATCC 33591	>64	4	4
JE2	>64	8	4
VRS1	>64	>64	4

tolerant MRSA cells treated with PQ401. These results indicate that PQ401 can cause membrane damage regardless of growth states.

To further explore the effects of PQ401 on bacterial lipid bilayers, we challenged biomembrane-mimicking giant unilamellar vesicles (GUVs) with PQ401. GUVs are artificial spherical vesicles made up of a single lipid bilayer with a diameter of 10 to 100 μm (38, 39). Their relatively large size enables direct observation of dynamic morphological changes by optical microscopy (40, 41). GUVs have been employed to investigate the modes of action of several membrane-active antibacterial agents, including daptomycin (38, 42–45). To mimic the negatively charged *S. aureus* membrane, we created GUVs consisting of a dioleoyl-*sn*-glycero-3-phosphocholine (DOPC)/1,2-dioleoyl-*sn*-glycero-3-phospho-(1'-*rac*-glycerol) (DOPG) lipid bilayer at a ratio of 7:3, which have been used for monitoring the effects of daptomycin and other membrane-active antimicrobial agents on *S. aureus* lipid bilayers (38, 46–49). When GUVs were treated with 4 $\mu\text{g/ml}$ ($1 \times \text{MIC}$) PQ401, we noted the formation of lipid aggregates on the surface of the GUVs after ~ 45 s, followed by rupture at ~ 100 s (Fig. 2B; see also Movies S1 and S2 in the supplemental material), indicating that PQ401 directly interacts with and disrupts bacterial mimetic lipid bilayers.

Membrane-active agents typically interact with both bacterial and mammalian lipid bilayers. To test the membrane selectivity of PQ401, we fabricated GUVs consisting of 1-palmitoyl-2-oleoyl-glycero-3-phosphocholine (POPC) and cholesterol in the ratio of 7:3, which mimics mammalian lipid bilayers (50, 51). In contrast to the bacterial mimetic GUVs, PQ401 did not induce any deformation of the mammalian mimetic GUVs at 4 $\mu\text{g/ml}$ or 10 $\mu\text{g/ml}$ (Fig. 2B and Movies S3 to S5). The inertness of mammalian membranes to PQ401 was confirmed using human erythrocytes. As shown in Fig. 2C, PQ401 did not induce detectable hemolysis of erythrocytes up to 512 $\mu\text{g/ml}$. Consistent with these results, PQ401 was previously reported to kill cancer cells by IGF-1R inhibition-mediated apoptosis rather than membrane disruption (28, 52). Combined, these results indicate that PQ401 has a high level of selectivity for bacterial in comparison to mammalian membranes.

Neutral PQ401 penetrates into bacterial lipid bilayers. To further explore the molecular details by which PQ401 interacts with bacterial membranes, we conducted all-atom molecular dynamics (MD) simulations. The topology and parameters of PQ401 for the GROMOS54a7 forcefield (53) were generated by Automated Topology Builder (ATB) (54, 55). Like bacterial membrane-mimetic GUVs, we used the previously established model of DOPC/DOPG at a 7:3 ratio to simulate negatively charged *S. aureus* membranes. The MD modeling showed that PQ401 is initially recruited to the mem-

TABLE 3 MICs of PQ401 against the ESKAPE pathogens

Strain	MIC ($\mu\text{g/ml}$) of drug:			
	PQ401	Vancomycin	Gentamicin	Ciprofloxacin
<i>Enterococcus faecium</i> E007	4	1	>64	>64
<i>Enterococcus faecium</i> C68	4	64	>64	>64
<i>Staphylococcus aureus</i> Newman	4	2	2	0.25
<i>Klebsiella pneumoniae</i> WGLW2	>64	>64	1	0.031
<i>Acinetobacter baumannii</i> ATCC 17978	>64	>64	1	0.25
<i>Pseudomonas aeruginosa</i> PA14	>64	>64	2	0.063
<i>Enterobacter aerogenes</i> ATCC 13048	>64	>64	2	0.031

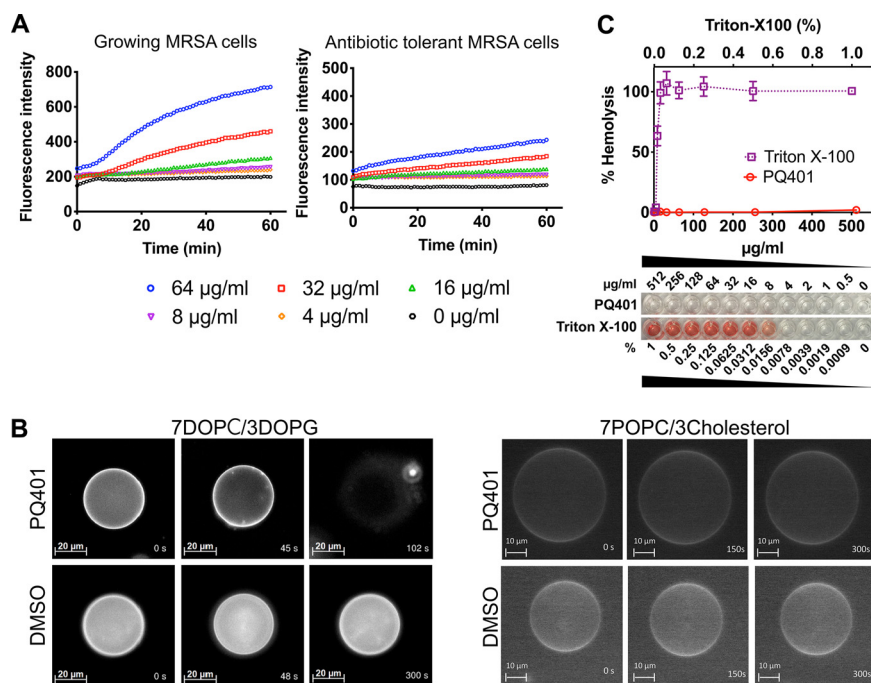


FIG 2 PQ401 selectively disrupts MRSA membranes. (A) Elicitation of membrane permeability by PQ401 for growing MRSA cells or stationary-phase antibiotic-tolerant MRSA cells. Membrane permeability was evaluated by monitoring the uptake of the membrane-impermeable dye SYTOX Green for 60 min. Results are shown as means from triplicates. Error bars (SD) are excluded for clarity. (B) GUVs consisting of DOPC/DOPG (7:3) or POPC/cholesterol (7:3) labeled with 0.05% Liss Rhod PE were treated with 4 $\mu\text{g/ml}$ PQ401 or 0.1% DMSO. Deformation dynamics of GUVs was monitored over time using fluorescence microscopy. (C) Two percent human erythrocytes were treated with a range of PQ401 concentrations for 1 h at 37°C. A sample treated with 1% Triton X-100, which causes 100% hemolysis, was used as the positive control. Results are shown as means \pm SD ($n = 3$).

brane surface by the binding of the chloro-methoxyphenyl moiety to hydrophilic lipid heads via the polar interactions between two polar moieties, including the urea and chloro-methoxyphenyl groups and hydrophilic lipid head groups (Fig. 3A; see also Fig. S1A and Movie S6). After several tens of nanoseconds of sustained attachment, PQ401 penetrates into the membrane interior, maximizing interactions between a nonpolar benzene ring and hydrophobic lipid tails (Fig. 3A and B and Movie S6). Potential mean force (PMF) calculations (Fig. S1B) using the umbrella sampling method (56) confirmed that insertion of PQ401 into the lipid bilayer is energetically favorable with a transfer energy about $-10 k_B T$ (Fig. 3C).

Next, we also conducted MD simulations to explore PQ401 interaction with the mammalian mimetic lipid bilayer of POPC-cholesterol at a 7:3 ratio. Unexpectedly, we found that the MD simulations predicted that PQ401 could also penetrate into the mammalian membrane with a slightly higher transfer energy than with the bacterial mimetic membrane (Fig. S1C). Although this simulation indicates that the penetration of PQ401 into mammalian lipid bilayers is energetically favorable, as described above, human red blood cells as well as GUVs having the same composition of POPC-cholesterol as the membranes used in the MD simulations (Fig. 2B and C and Movies S3 to S5) are resistant to disruption by PQ401. Combined, these data indicate that the penetration of PQ401 molecules *per se* is not sufficient to induce the disruption of mammalian lipid bilayers.

The ionization states of PQ401 can be varied. The MarvinSketch program (ChemAxon Ltd.) predicts that PQ401 has 4 different ionization states: a neutral, a protonated, and two deprotonated forms at the ratios of 98.48 to 1.45 to 0.06 to 0.02, respectively, at pH 7.4 (Fig. 3A; Table 4). To address whether the ionization state affects membrane activity, we conducted additional MD simulations. In contrast to the neutral

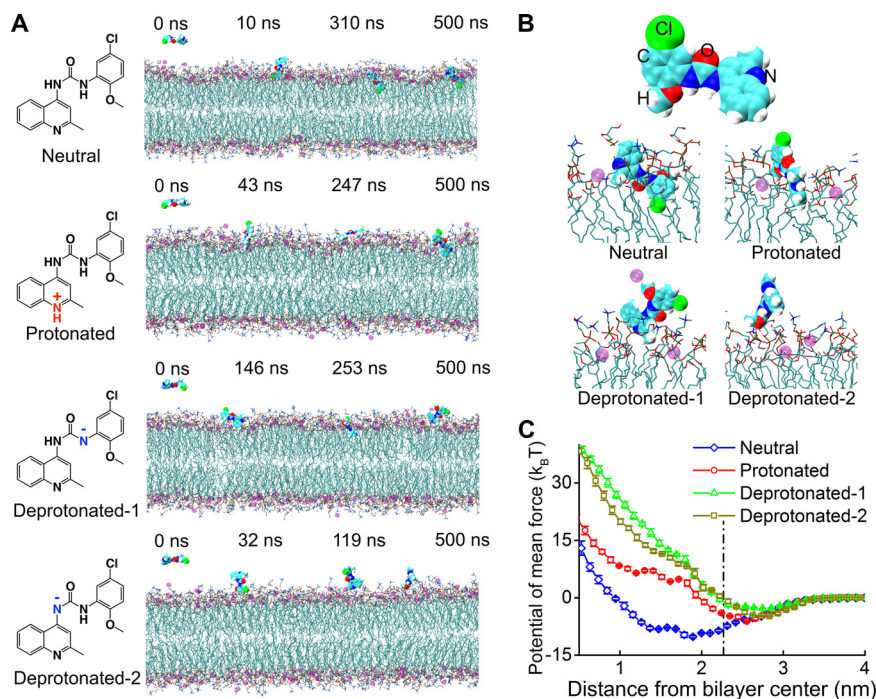


FIG 3 Only the neutral form of PQ401 is predicted to penetrate into bacterial lipid bilayers. (A) Representative simulated configurations of PQ401 in different ionized states from left to right: onset, membrane attachment, membrane penetration, and equilibrium interacting with 7DOPC/3DOPG lipid bilayers. PQ401 and sodium ions are depicted as large spheres; phospholipids are represented as chains. The atoms in PQ401, phospholipids, and sodium ions are colored as follows: hydrogen, white; oxygen, red; nitrogen, blue; chlorine, green; carbon, cyan; phosphorus, orange; sodium, purple. Water molecules are not shown for clarity. (B) Magnified view of PQ401 and the corresponding simulated configurations at 500 ns in different ionized states. (C) The free energy profiles of PQ401 in different ionized states penetrating into the lipid bilayer as a function of the center-of-mass (COM) distance to the bilayer. The dot-dashed black line marks the surface of the membrane, averaged from the COM locations of phosphate groups in the lipids of the outer leaflet. Error bars represent means \pm SD from three independent simulations.

form, the penetration of all three of the ionized forms into lipid bilayers was not energetically favorable (Fig. 3C). The mechanisms by which each of the ionized forms interacts with lipid bilayers are somewhat different. In the case of the protonated form, unlike the neutral form, the positively charged methylquinoline group instead of the chloro-methoxyphenyl moiety drives the molecule to the negatively charged surface of the lipid bilayer; however, the strong binding between the positively charged methylquinoline group and the negatively charged membrane surface prevents further penetration (Fig. 3A and B, Fig. S1A, and Movie S7). In the case of two deprotonated forms, like the neutral form, the chloro-methoxyphenyl moiety binds on the surface of the bilayer membrane; however, it is unable to penetrate into lipid bilayers because of the electrostatic repulsion between the negatively charged nitrogen and negatively charged lipid head groups (Fig. 3A and B, Fig. S1B, and Movies S8 and S9).

TABLE 4 Proportion of each ionized form of PQ401 and their MICs against MRSA strain MW2^a

pH	% ratio (N:P:Dp1:Dp2)	MIC ($\mu\text{g/ml}$) of drug:	
		PQ401	Vancomycin
5.5	46.15:53.85:0.00:0.00	16	1
6.5	89.54:10.45:0.01:0.00	4	1
7.4	98.48:1.45:0.06:0.02	4	1
8.5	98.96:0.12:0.72:0.02	4	1

^aAbbreviations: N, neutral form; P, protonated form; Dp1, deprotonated-1 form; Dp2, deprotonated-2 form shown in Fig. 3. Ionized states were estimated by MarvinSketch.

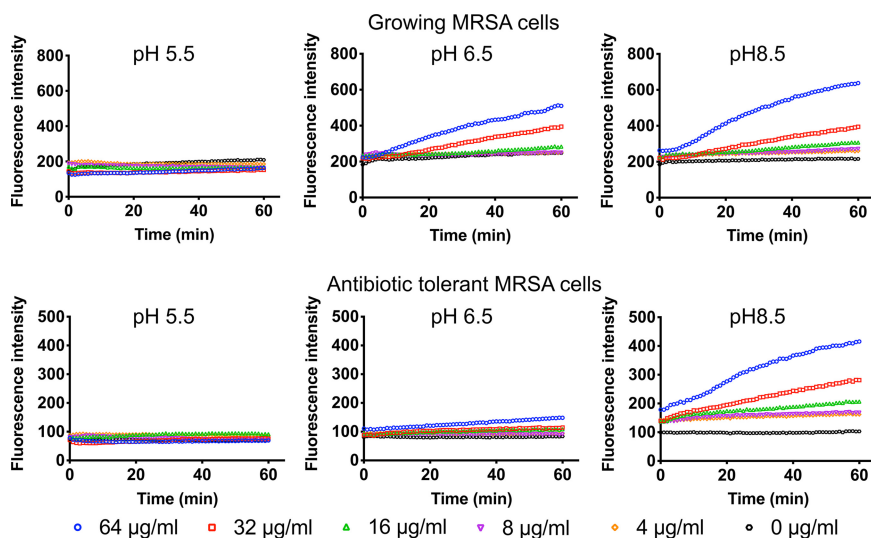


FIG 4 The membrane permeability of PQ401 is augmented as pH increases. Membrane permeability by PQ401 at the indicated pH was evaluated by monitoring the uptake of SYTOX Green for 60 min. Results are shown as means from triplicates. Error bars (SD) are excluded for clarity.

To verify these MD simulation results experimentally, we decreased the portion of the neutral PQ401 by lowering the pH. The MarvinSketch program predicts that at pH 5.5, more than 50% of PQ401 exists in a protonated form, which, according to the MD simulations, is unable to penetrate the membrane (Table 4 and Fig. 3). Consistent with the MD simulations, the MIC of PQ401 at pH 5.5 increased to 16 µg/ml, which is 4-fold higher than at pH 7.4 (Table 4). Further, the ability of PQ401 to permeabilize the membrane of both growing and nongrowing antibiotic-tolerant MRSA was significantly decreased at pH 5.5 (Fig. 4). As pH increased, the membrane permeability of PQ401 also increased (Fig. 4). Between pH 6.5 and 8.5, the MIC of PQ401 was 4 µg/ml, where the neutral portion of PQ401 is 90% or greater. These computational and experimental results demonstrate that the polarity of branch groups, the hydrophobicity of core rings, and the ionization state play important roles in the membrane activity of PQ401.

PQ401 kills antibiotic-tolerant MRSA and shows synergism with gentamicin. As shown above, PQ401 induces membrane permeabilization of antibiotic-tolerant MRSA cells (Fig. 2A). Thus, we reasoned that PQ401 should be effective against antibiotic-tolerant MRSA. As previously reported and shown here in Fig. 5A, 100% of stationary-phase MRSA cells become antibiotic-tolerant cells that are not susceptible to a panel of antibiotics having different modes of action. Indeed, PQ401 showed bactericidal activity

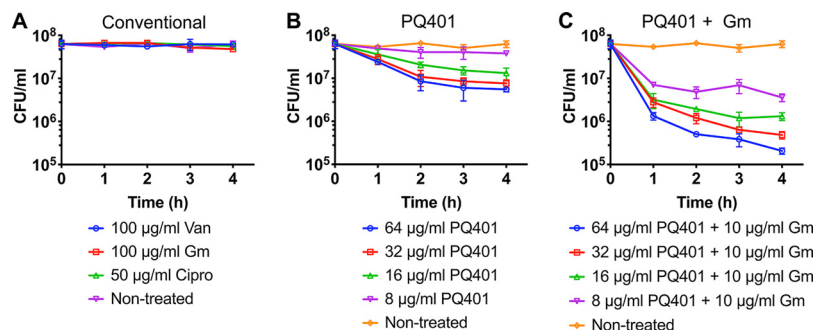


FIG 5 PQ401 has bactericidal potency and shows synergism with gentamicin against antibiotic-tolerant MRSA. Antibiotic-tolerant cells of MRSA MW2 were treated with 100× MIC vancomycin (Van), gentamicin (Gm), or ciprofloxacin (Cipro) (A); the indicated concentrations of PQ401 (B); or 10 µg/ml gentamicin (Gm) in combination with various concentrations of PQ401 for 4 h (C). CFU counts of viable cells were measured by serial dilution and plating on TSA plates. Results are shown as means ± SD ($n = 3$).

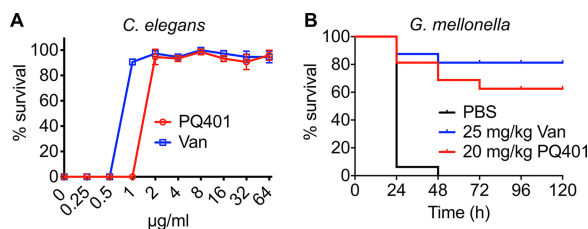


FIG 6 PQ401 shows efficacy in two invertebrate animal infection models. (A) MRSA-infected *C. elegans* *glp-4(bn2);sek-1(km4)* animals were treated with the indicated concentrations of PQ401 or vancomycin at 25°C for 5 days. After staining dead worms with SYTOX Orange, percent survival of *C. elegans* was calculated in each well of the assay plate. Results are shown as means \pm SD ($n = 3$). (B) Sixteen MRSA-infected *G. mellonella* larvae ($n = 16$) were treated with control (PBS), 25 mg/kg vancomycin (Van), or 20 mg/kg PQ401 at 1 h postinfection. Larval survival following treatment with 20 mg/kg PQ401 was significant compared to PBS treatment ($P < 0.0001$). Data are representative of two independent experiments.

against antibiotic-tolerant MRSA cells in a dose-dependent manner, albeit with significantly less activity than against growing MRSA. PQ401 caused a 1-log reduction in antibiotic-tolerant MRSA viability at 64 $\mu\text{g/ml}$ ($4\times$ MIC) (Fig. 5B).

Membrane-active antimicrobial agents are known to act synergistically with aminoglycosides against antibiotic-tolerant bacteria by facilitating the diffusion of the aminoglycoside across bacterial membranes (6, 20, 21, 57). We tested the synergism of PQ401 with the aminoglycoside antibiotic gentamicin against antibiotic-tolerant MRSA cells. As shown in Fig. 5C, combined with gentamicin, the bactericidal activity of PQ401 was enhanced against antibiotic-tolerant MRSA. The combination of 64 $\mu\text{g/ml}$ PQ401 and 10 $\mu\text{g/ml}$ gentamicin led to a ~ 3 -log reduction in antibiotic-tolerant MRSA viability (Fig. 5C).

PQ401 is efficacious in invertebrate animal models. To test the efficacy of PQ401, we used two invertebrate model hosts, *C. elegans* and *Galleria mellonella* (wax moth) larvae. These two infection models are widely used to evaluate *in vivo* antimicrobial potential and toxicity, which can fill the gap between *in vitro* and *in vivo* mammalian experiments (29, 30, 58). In a *C. elegans*-MRSA infection model, PQ401 exhibited a median effective concentration (EC_{50}) of 1.7 $\mu\text{g/ml}$, which is ~ 2 -fold higher than the EC_{50} (0.86 $\mu\text{g/ml}$) of vancomycin (Fig. 6A). PQ401 completely blocked *C. elegans* death from MRSA infection at ~ 2 $\mu\text{g/ml}$, which, interestingly, is ~ 2 -fold lower than its MIC of 4 $\mu\text{g/ml}$, whereas vancomycin provided 100% worm survival at around the MIC. In addition, the exposure of MRSA-infected *C. elegans* at 64 $\mu\text{g/ml}$ PQ401 for 5 days did not affect *C. elegans* viability (Fig. 6A).

Next, we tested the efficacy of PQ401 in *G. mellonella* larvae. All MRSA-infected *G. mellonella* larvae were dead within 48 h postinfection. We treated the infected larvae with 20 mg PQ401/kg of body weight by injecting 10 μl of 0.5 mg/ml PQ401, which is the maximum injectable dose due to its solubility in phosphate-buffered saline (PBS). Also, PQ401 does not cause hemolysis at this concentration of 0.5 mg/ml (Fig. 2C). The PQ401-treated larvae showed 62.5% survival at 120 h postinfection (Fig. 6B), indicating significant efficacy ($P < 0.0001$, Fig. 6B). Consistent with MIC and EC_{50} results (Table 1 and Fig. 6A), PQ401 efficacy was lower than vancomycin, showing 81.5% survival at 120 h postinfection (Fig. 6B). Taken together, PQ401 is significantly efficacious in the two MRSA infection animal models.

DISCUSSION

Major disadvantages of conventional antibiotics include resistance development and inactivity against nongrowing antibiotic-tolerant bacteria. Ideally, the targets of a new generation of antibiotics should be growth independent and pathogens should exhibit very low rates of resistance development to antimicrobials corresponding to these targets. Membrane-disruptive antimicrobial agents have a potential to overcome the drawbacks of conventional antibiotics if they exhibit membrane selectivity to

bacterial compared to mammalian membranes (14, 59). PQ401 is a new example of a class of membrane-active agents that we have recently described that exhibit antimicrobial potency against multidrug-resistant and multidrug-tolerant *S. aureus*, low probability for the development of resistance, and the ability to act synergistically with other antibiotics as well as high membrane selectivity to Gram-positive bacterial membranes.

Interestingly, PQ401 rescued 100% of *C. elegans* worms from MRSA infections at one-half the MIC, whereas vancomycin rescued 100% only at $1\times$ MIC (Fig. 6A), indicating that PQ401 may provide additional beneficial bioactivity to combat MRSA infections. PQ401 may suppress the expression of MRSA virulence at subinhibitory concentrations. Several antibiotics, such as linezolid and tigecycline, have been shown to reduce *S. aureus* virulence factor expression at sub-MIC levels (60). Also, our laboratory reported previously that a different membrane-active antimicrobial, NH125, downregulated the expression of several virulence factors, including alpha-hemolysin, delta-hemolysin, coagulase, and nuclease, at subinhibitory concentrations (61). At sub-MIC levels, antibacterial compounds targeting protein synthesis may decrease virulence gene expression (60), and subinhibitory concentrations may also act as a selective pressure for resistant development (62). However, since PQ401 displays a very low probability for resistance development at sub-MIC levels, it is possible that its antivirulence activity at subinhibitory concentrations could contribute to its ability to treat MRSA infections.

The design and development of membrane-active small molecules have been traditionally based on a strategy that involves mimicking natural AMPs secreted from a variety of host organisms, including both plant and animal species, because their membrane selectivity and antimicrobial activity have been optimized through evolution in nature (63, 64). In general, common features of AMPs include a net charge of $\sim +3$ and a hydrophobic content of $\sim 42\%$ (15, 65, 66). Arginine and lysine are responsible for the cationic characteristics; tryptophan, phenylalanine, leucine, and isoleucine contribute to hydrophobicity (63). In particular, the cationic nature of AMPs plays a key role in selective binding to negatively charged bacterial membranes rather than to zwitterionic mammalian membranes (15, 63). Following an initial electrostatic interaction with a bacterial membrane, the hydrophobic residues of AMPs interact with bacterial lipid tails (15, 63). Based on this paradigm, rationally designed membrane-active small molecules usually exhibit cationic and amphipathic structures (15, 16) and have a similar mode of action as AMPs. Interestingly, although daptomycin, an FDA-approved membrane-active and last-resort antibacterial against MRSA, is anionic, it forms a cationic complex with Ca^{2+} and therefore uses electrostatic attraction to interact with negatively charged bacterial membranes similarly to AMPs (67).

A disadvantage of cationic AMPs and cationic low-molecular-weight compounds as antimicrobial therapeutics is that the electrostatic binding of cationic antimicrobials to anionic bacterial membranes can result in the selection of AMP-resistant bacteria that exhibit an overall reduced negative charge (17, 18). Such mutants often exhibit cross-resistance to a broad spectrum of cationic membrane-active antimicrobials, which includes daptomycin (18). Moreover, AMP-resistant bacteria are potentially also more resistant to host innate immunity-related effectors such as defensins and cathelicidins that target bacterial membranes (18). For example, daptomycin-resistant *S. aureus* strains exhibit cross-resistance to host defense peptides including human neutrophil defensin-1 and LL-37 (68, 69).

In contrast to conventional membrane-active antimicrobial small molecules and peptides, the membrane activity of PQ401 is maximized when it exists in a neutral form rather than a cationic form (Fig. 3). Furthermore, PQ401 does not have clear lipophilic elements, such as acyl chains. In the case of PQ401, two polar moieties, the chloromethoxyphenyl and urea groups, provide sufficient affinity to bind PQ401 to the surface of the lipid bilayer. Importantly, this attraction of the chloromethoxyphenyl group to the membrane surface is not so strong that it hinders further penetration of PQ401 and subsequent interaction with hydrophobic lipid tails (Fig. 3; see also Movie S6 in the supplemental material). In light of the development of cross-resistance to cationic

membrane-active compounds, neutral antimicrobial membrane-targeting compounds such as PQ401 should circumvent this issue.

To date, we have described four different classes of small-molecule membrane-active agents including NH125 (19, 49), synthetic retinoids (CD437, CD1530) (20), nTZDpa (21), and bithionol (6) that are effective against antibiotic-tolerant MRSA cells. Except for NH125, which is cationic and amphipathic, the remaining three compounds, as well as PQ401, are neither cationic nor amphipathic but also exhibit significant differences from each other. CD437 and nTZDpa have a carboxylic moiety and predominately exist as a negatively charged deprotonated form at pH 7.4. According to predictions made using MarvinSketch, more than 50% of bithionol also exists as anionic forms at pH 7.4. Previously, our laboratory reported MD simulations which show that the neutral forms of CD437, nTZDpa, and bithionol penetrate into lipid bilayers (6, 20, 21). Our working hypothesis is that their anionic forms probably have significantly reduced membrane activity due to electrostatic repulsion to negatively charged bacterial membranes as shown in the case of anionic forms of PQ401 (Fig. 3).

Unlike PQ401, however, only relatively small portions of the neutral forms of CD437, nTZDpa, and bithionol exist at pH 7.4. The reason why CD437, nTZDpa, and bithionol are such effective membrane disrupters at neutral pH is not understood, but one possibility is that the neutral forms of these molecules accumulate over time in bacterial membranes, ultimately reaching high-enough concentrations to disrupt membrane function. From a kinetic point of view, embedment of these neutral molecules into bacterial membranes is very fast (within hundreds of nanoseconds), energetically favorable, and almost irreversible (Fig. 3A and C and Movie S6) (6, 20, 21). Once embedded, the energy cost ($\sim 10 k_B T$) to remove these molecules from the membranes is high (Fig. 3C) (6, 20, 21). Further, at physiological pH, the ratio of anionic and neutral forms of these molecules in solution remains constant to satisfy the Henderson-Hasselbach equation ($\text{pH} = \text{pK}_a + \log_{10} [\text{A}^-]/[\text{HA}]$). Thus, because only a small portion of these molecules are present in a neutral form at physiological pH, as neutral forms are embedded into the membranes, more neutral forms are generated from anionic forms to essentially maintain a constant concentration of neutral molecules outside the bacteria (70). In any case, cationic forms of CD437, nTZDpa, or bithionol do not exist at any physiological pH. Therefore, CD437, nTZDpa, and bithionol as well as PQ401 demonstrate that unconventional small molecules can bind to and disrupt negatively charged bacterial membranes in a cationic-independent manner.

Although PQ401 did not cause either disruption of the mammalian mimetic GUVs or lysis of human red blood cells at concentrations up to 512 $\mu\text{g}/\text{ml}$ (Fig. 2B and C and Movies S3 to S5), the MD simulations predicted that PQ401 could penetrate into simulated mammalian lipid bilayers (Fig. S1C), suggesting that there is a discrepancy between the MD simulation and experimental results. However, it is important to point out that the all-atom MD simulations evaluate only the ability of a single molecule to penetrate a lipid bilayer based on free energy profiles. In contrast, our previous studies showed that at least three factors including a molecule's ability to attach to, penetrate, and perturb membrane lipid bilayers play important roles in membrane disruption (6, 20, 21). Thus, our current data with PQ401 suggest that it is possible that the collective behavior of a group of molecules rather than the behavior of single molecules is required for the disruption of lipid bilayers. For example, groups of interacting daptomycin molecules form oligomeric pores in bacterial lipid bilayers that induce membrane disruption (67). Moreover, the physical properties of particular lipid bilayers confer different levels of resistance to disruption to membrane-penetrating compounds. The 7POPC/3Cholesterol bilayer is much stiffer (over $100 k_B T$) than the 7DOPC/3DOPG ($\sim 20 k_B T$) bilayer (71). Therefore, it is not unexpected that simulations of the interaction between a single molecule and a lipid bilayer do not reflect all of the features observed in our wet-lab experiments with GUVs and red blood cells.

Despite the attractive properties of PQ401 as a potential lead compound for the development of an antimicrobial therapeutic, PQ401 has limitations that require further development. First, PQ401 was identified as an inhibitor of IGF-1R that induces the

apoptosis of a variety of cancer cells by blocking the autophosphorylation of IGF-1R (28, 52). IGF-1R plays important roles in several cellular processes, including cell proliferation, development, and survival. Dysregulation of IGF-1R results in many diseases, including cancers, thyroid eye disease, psoriasis, and diabetes (72). Therefore, for the further development of PQ401 as an antimicrobial therapeutic, it would be critical to minimize potential toxic side effects of PQ401 by nullifying its IGF-1R-inhibitory activity while maintaining its antimicrobial activity. Second, the MIC of PQ401 is 4 $\mu\text{g/ml}$ against proliferating MRSA MW2 cells (Table 1), which is 4-fold higher than the MIC ($\sim 1 \mu\text{g/ml}$) of vancomycin, daptomycin, and linezolid (6, 20), which are currently used to treat MRSA infections. Moreover, PQ401 treatment of nongrowing antibiotic-tolerant MRSA at 64 $\mu\text{g/ml}$ resulted in only a 10-fold decrease in viability (Fig. 5B), whereas other membrane-active antimicrobials recently identified in our laboratory, such as particular synthetic retinoids, nTZDpa, and bithionol, completely eradicated antibiotic-tolerant MRSA at this concentration (6, 20, 21). Finally, PQ401 exhibits poor aqueous solubility. In the case of the *G. mellonella* larva infection model, 20 mg/kg was the maximum dose possible.

Fortunately, however, it seems likely that it should be feasible to eliminate the IGF-1R-inhibitory activity of PQ401 as well as improve its antimicrobial activity and aqueous solubility and decrease its toxicity by appropriate structural modifications. First of all, the crystal structure of IGF-1R has been determined (73). Based on this structural information, the interactions between IGF-1R and small-molecule inhibitors are well defined, and extensive *in silico* molecular docking analyses have been carried out (74–76). Combining what is known about the well-defined interaction mechanism between small molecules and IGF-1R with our data pertinent to the penetration of PQ401 into Gram-positive bacterial lipid bilayers, it seems likely that it would be possible to eliminate the IGF-1R-inhibitory activity of PQ401 without the loss of its bacterial membrane-disrupting activity. In this regard, it is noteworthy that replacement of a carboxyl acid with a primary alcohol in the synthetic retinoid CD437 results in a significant reduction of its anticancer activity while maintaining its antimicrobial activity (20).

In addition, based on structure-activity relationship (SAR) studies on synthetic retinoids, we found that the deep penetration of bulky moieties leads to improved antimicrobial activity by enhanced membrane perturbation (20). In the case of nTZDpa, we found that additional halogen substituents and the replacement of chlorine with a larger halogen atom such as iodine significantly enhance antimicrobial activity against both growing and nongrowing antibiotic-tolerant MRSA as well as membrane selectivity for bacterial over mammalian membranes (21). Based on these SAR results, we think the addition of halogen atoms or substitution of larger halogen atoms for chlorine may augment PQ401's antimicrobial activity. In addition, the SAR studies of diarylurea derivatives aiming at improving biological activity, aqueous solubility, and bioavailability have been intensively conducted and their synthetic procedures are well established (24–26, 77–79). Therefore, the established SAR of diarylurea derivatives coupled with the molecular mechanisms described in this study provides a strong rationale for further optimization of PQ401 as a potential membrane-active antibiotic.

In conclusion, we discovered that PQ401 is a potent antimicrobial that is effective against both multidrug-resistant and multidrug-tolerant *S. aureus*. PQ401 kills bacteria by selectively disrupting bacterial lipid bilayers, exhibits relatively strong bactericidal activity against growing MRSA cells, has a low probability of selecting for resistance, exhibits synergism with gentamicin against antibiotic-tolerant MRSA, and shows significant efficacy against MRSA in both *C. elegans* and *G. mellonella* infection models. Finally, unlike cationic antimicrobial agents, the antimicrobial activity of PQ401 is maximized when it exists in its neutral form. This feature of PQ401 in comparison to cationic antimicrobial peptides significantly expands the potential diversity of membrane-active antimicrobial agents.

MATERIALS AND METHODS

Bacterial strains and growth conditions. Methicillin-susceptible *S. aureus* strain Newman (80); methicillin-resistant *S. aureus* (MRSA) strains MW2 BAA-1707 (81) ATCC 33591, and JE2 (82); vancomycin-resistant *S. aureus* strain VRS1 (32); 11 clinical *S. aureus* isolates (49); *Enterococcus faecium* E007 (83, 84); vancomycin-resistant *E. faecium* strain C68 (34, 85); *Klebsiella pneumoniae* WGLW2 (BEI Resources, Manassas, VA, USA); *Acinetobacter baumannii* ATCC 17978 (86); *Pseudomonas aeruginosa* PA14 (87); and *Enterobacter aerogenes* ATCC 13048 were used to test antimicrobial activity (Tables 1 to 3). *S. aureus* strains were grown in tryptic soy broth (TSB) (BD, Franklin Lakes, NJ, USA), and *E. faecium* strains were grown in brain heart infusion (BHI) broth (BD, Franklin Lakes, NJ, USA) at 37°C at 200 rpm. *K. pneumoniae*, *A. baumannii*, *P. aeruginosa*, and *E. aerogenes* were grown in Luria-Bertani (LB) broth (BD, Franklin Lakes, NJ, USA) at 37°C at 200 rpm.

Antimicrobial agents and chemicals. Vancomycin, oxacillin, gentamicin, and ciprofloxacin were purchased from Sigma-Aldrich (St. Louis, MO, USA). PQ401 was purchased from R&D Systems (Minneapolis, MN, USA). Stocks of all antibiotics of 10 mg/ml were made in dimethyl sulfoxide (DMSO) or double-distilled water (ddH₂O).

MIC and MBC assays. The MICs of antibiotics were determined by the standard microdilution method recommended by the Clinical and Laboratory Standards Institute (88). The pH of the medium (cation-adjusted Mueller-Hinton broth) was adjusted to the desired values with NaOH or HCl, and then the media were filter sterilized through 0.22- μ m-pore-size membrane filters. The MBC of PQ401 was determined by identifying the lowest concentration that killed $\geq 99.9\%$ (3 logs) of an initial bacterial inoculum (5×10^5 CFU/ml) in 24 h (89). CFU were determined by serial dilution and spot-plating on tryptic soy agar (TSA) plates. MIC and MBC assays were conducted in triplicate.

Killing kinetics assay. An *S. aureus* overnight culture was diluted 1:10,000 in 25 ml fresh TSB in a 250-ml flask. In order to obtain exponential-phase cells, the diluted cell suspension was incubated at 37°C with shaking at 225 rpm for 4 h until the optical density at 600 nm (OD₆₀₀) reached 0.4 ($\sim 2 \times 10^7$ CFU/ml). One milliliter of the exponential-phase cell culture was added to the wells of a 96-well assay block (Corning Costar 3960) containing 1 ml of prewarmed TSB with twice the desired concentrations of compounds. The assay block was sealed with a gas-permeable membrane (Breathe-Easy; Diversified Biotech) and was incubated at 37°C shaking at 200 rpm. At hourly intervals, 400- μ l aliquots were taken, washed once with PBS, serially diluted, and spot-plated onto tryptic soy agar (TSA; BD) plates. After incubation at 37°C overnight, the number of cells was calculated based on colony count. These experiments were conducted in triplicate.

Resistance selection. Development of resistant mutants by serial passage was conducted as previously described (36). Briefly, an extended range of titers of PQ401 was generated by 2-fold serial dilution with cation-adjusted Mueller-Hinton (CaMH) broth (Difco, Detroit, MI, USA) from three different starting concentrations (20, 24, and 32 μ g/ml) covering 0.1875 to 32.0 μ g/ml. Three sets of an extended gradient of PQ401 titers were created in a 96-well plate to provide triplicates for the experiment. The same extended range of concentrations of ciprofloxacin was used as a positive control. MRSA MW2 overnight cultures were adjusted to 1×10^6 CFU/ml in CaMH broth, and 50 μ l of the diluted cultures was dispensed into the 96-well plates containing 50 μ l of the extended gradient of antibiotics. After incubating the plate at 37°C for 24 h, OD₆₀₀ was measured by a spectrophotometer (SpectraMax M2; Molecular Devices). Bacterial growth was defined as OD₆₀₀ of ≥ 0.1 . Bacterial culture at the highest drug concentration that permitted bacterial growth was diluted 1,000-fold in CaMH, and the diluted culture was then used as inoculum for the next passage. The rest of the culture was stored in 16% glycerol at -80°C . This process was repeated for 25 days.

Antibiotic-tolerant MRSA-killing assay. As previously demonstrated, 100% of *S. aureus* cells in a liquid culture become antibiotic-tolerant cells when grown to stationary phase (3–5, 8). Consistently, we have shown previously that when grown to stationary phase, MRSA MW2 is tolerant to conventional antibiotics such as gentamicin, ciprofloxacin, vancomycin, linezolid, and daptomycin (6, 19–21). The antibiotic-tolerant cells of MRSA MW2 were prepared by growing cultures overnight to stationary phase at 37°C at 200 rpm and washing three times with PBS. One milliliter of $\sim 1 \times 10^8$ CFU/ml antibiotic-tolerant MRSA cells was added to 1 ml of PBS containing a 2-fold-higher concentration of the desired concentration of antibiotics in a 96-well assay block (Corning Costar 3960). One milliliter of the antibiotic-tolerant MRSA cell suspension containing appropriate concentrations of antibiotics was added to the wells of a 2-ml deep-well assay block (Corning Costar 3960) and incubated at 37°C, with shaking at 225 rpm. At every hour, 400- μ l samples were removed, washed once with PBS, serially diluted, and spot-plated on TSA plates. Colonies were counted after overnight incubation at 37°C to determine the titer of live cells. These experiments were conducted in triplicate.

SYTOX Green membrane permeability assay. The pH of phosphate-buffered saline (PBS) was adjusted to the desired values with NaOH or HCl, and then the PBS was filter sterilized through 0.22- μ m-pore-size membrane filters. Black, clear-bottom, 96-well plates (Corning no. 3904) were filled with 50 μ l of PBS/well containing the indicated concentration of antibiotics. Exponential-phase or stationary-phase antibiotic-tolerant *S. aureus* MW2 cells prepared as described under “Killing kinetics assay” and “Antibiotic-tolerant MRSA-killing assay,” respectively, were then washed 3 times with the same volume of PBS. The washed cells were adjusted to an OD₆₀₀ of 0.4 ($\sim 2 \times 10^7$ CFU/ml) with PBS. SYTOX Green (Molecular Probes) was added to 10 ml of the diluted bacterial suspension to a final concentration of 5 μ M and incubated for 30 min at room temperature in the dark. Fifty microliters of the bacterium-SYTOX Green mixture was added to each well of the 96-well plates containing antibiotics. Fluorescence was measured at room temperature using a spectrophotometer (SpectraMax M2; Molecular Devices) at the excitation of 485 nm and the emission of 525 nm. All experiments were conducted in triplicate.

Preparation of GUVs and observation of effects of compounds on GUVs. Giant unilamellar vesicles (GUVs) were prepared by the electroformation method described previously (6) with slight modifications. 1,2-Dioleoyl-*sn*-glycero-3-phosphocholine (DOPC), 1,2-dioleoyl-*sn*-glycero-3-phospho-(1'-*rac*-glycerol) (DOPG), 1-palmitoyl-2-oleoyl-glycero-3-phosphocholine (POPC), cholesterol (ovine wool), and 1,2-dioleoyl-*sn*-glycero-3-phosphoethanolamine-*N*-(lissamine rhodamine B sulfonyl) (18:1 Liss Rhod PE) were purchased from Avanti Polar Lipids (Alabaster, AL, USA). Lipid mixtures of 4 mM consisting of DOPC-DOPG-18:1 Liss Rhod PE (7:3:0.005) and POPC-cholesterol-18:1 Liss Rhod PE (7:3:0.005) were dissolved in chloroform, respectively. The procedure for electroformation of both types of GUVs (7DOPC/3DOPG and 7POPC/3cholesterol) was the same. Indium tin oxide (ITO)-coated slides (50 × 75 × 1.1 mm; Delta Technologies, Loveland, CO, USA) were coated with 20 μl of the lipid mixture and dried in a vacuum chamber for 2 h to remove chloroform. An electroformation chamber was made by placing a 2-mm-thick Teflon spacer between the two lipid-coated ITO slides. After adding 2 ml of 100 mM sucrose into the electroformation chamber, the chamber was sealed with binder clips and then connected to an AC field function generator. An AC field of 1.5-V voltage and 10-Hz frequency was applied for 2 h at room temperature, resulting in 10- to 50-μm-sized vesicles. The harvested GUV suspension was diluted (1:3) in a solution containing 1 volume of 100 mM sucrose and 6 volumes of 110 mM glucose. Forty-nine microliters of the diluted GUV suspension (~100 vesicles) was added into a black, clear-bottom 384-well plate (Corning no. 3712). The plate was left in the dark at room temperature for 15 min until all GUVs settled on the bottom of the plates. After adding 1 μl of compound solution to a well (final compound concentration, 1 × MIC), the GUVs were observed and imaged with an optical microscope equipped with fluorescence contrast and a digital camera (63× objectives; Axio Observer A1 and AxioCam MRm; Zeiss, Germany). Images and movies are representative of five independent experiments.

Human blood hemolysis. Ten percent human erythrocytes were purchased from Rockland Immunochemicals (Limerick, PA, USA). The erythrocytes were diluted to 4% with PBS, and 100 μl was added to 100 μl of 2-fold serial dilutions of compounds in PBS, 0.2% DMSO (negative control), or 2% Triton X-100 (positive control) in a 96-well plate. The 96-well plate was incubated at 37°C for 1 h and then centrifuged at 500 × *g* for 5 min. One hundred microliters of the supernatant was transferred to a fresh 96-well plate, and absorbance of supernatants was measured at 540 nm. Percent hemolysis was calculated using the following equation: $(A_{540} \text{ of compound-treated sample} - A_{540} \text{ of 0.1\% DMSO-treated sample}) / (A_{540} \text{ of 1\% Triton X-100-treated sample} - A_{540} \text{ of 0.1\% DMSO-treated sample}) \times 100$. All experiments were independently repeated 3 times using different batches of human erythrocytes.

All-atom MD simulations. All-atom MD simulations based on the GROMACS package (90) were performed to investigate the interactions between PQ401 or its different ionized forms and a simulated bacterial plasma membrane. The topologies and parameters of the compounds were generated by Automated Topology Builder (54, 55). The bacterial membrane was represented by a mixed lipid bilayer composed of 88 neutrally charged DOPC and 40 negatively charged DOPG lipids (~7:3 ratio) with Berger's lipid force field (91), which has been extensively used in previous studies (38, 46–48). Similarly to our previous studies (6, 20, 21), water was represented by the SPC/E model (92); a geometric combining rule was adopted for nonbonded interactions of the compounds with lipids, ions, and water (93, 94); the fast smooth particle-mesh Ewald method (95) was used to calculate the long-range electrostatic interactions; and sodium ions were added to neutralize the system. The simulation box had an initial size of 5.96 × 5.96 × 12.3 nm, which was large enough to prevent the compounds interacting with their periodic images. The system was modeled as an NPT ensemble (1 atm, 300 K) with periodic boundary conditions in all directions. The time step was 2 fs. After a 500-ns initial equilibration of solvated lipid systems, the compound was introduced into the water phase above the membrane. After 100 ns of reequilibration, the compound was released, and the system was further simulated for 500 ns (96). Additional simulations were performed to get the free energy profiles for the penetrations of compounds into the membrane, which were calculated by steered molecular dynamics (97), umbrella sampling, and the weighted histogram analysis methods (WHAM) (56, 98). In the sampling, the width of each window was 0.15 nm, each window was simulated for 25 ns, and the first 5 ns was discarded in the WHAM analysis.

C. elegans-MRSA liquid killing assay. The *C. elegans*-MRSA infection assay was conducted as described in a previous study (99). A *C. elegans glp-4(bn2);sek-1(km4)* double mutant strain was used for this assay. The *glp-4(bn2)* mutation blocks the production of progeny at 25°C (100), which prevents matricidal killing during the infection due to internal hatching of eggs (101). The *sek-1(km4)* mutation immunocompromises the worms and increases their sensitivity to infection, which reduces the assay time (102). The worms were maintained at 15°C on 10-cm slow-kill (SK) agar plates seeded with *Escherichia coli* HB101 (103). Eggs isolated from gravid adults by hypochlorite treatment were resuspended in M9 buffer and incubated with gentle rocking at 15°C for 48 h. Approximately 4,500 L1 hatchlings were placed on each SK plate seeded with HB101 for 52 h at 25°C until the animals grew into sterile young adults. The wells of a black, clear-bottom 384-well plate (Corning no. 3712) were filled with 20 μl M9 buffer including the desired concentrations of PQ401, vancomycin, or 1% DMSO (negative control). After adding 15 young adult *C. elegans glp-4(bn2);sek-1(km4)* animals to each well of the plate using a COPAS large particle sorter (Union Biometrica, MA, USA), 35 μl of MRSA MW2 suspension was added (OD₆₀₀ 0.08). The assay plate was sealed with a gas-permeable membrane (Breathe-Easy; Diversified Biotech, Dedham, MA, USA) and then incubated in a humidified chamber at 25°C for 5 days. After washing the plate 8 times with M9 buffer using a microplate washer (BioTek ELx405; BioTek, VT, USA), worms were stained with 0.7 μM SYTOX Orange. To evaluate worm survivability, the worms were imaged using an Image Xpress Micro automated microscope (Molecular Devices), capturing both transmitted light and tetramethyl rhodamine isocyanate (TRITC) (535-nm excitation, 610-nm emission)

fluorescent images with a 2× objective. Only dead worms are stained by SYTOX Orange. The assay was conducted in biological triplicate.

G. mellonella survival assays. Larvae were purchased from a commercial vendor (Vanderhorst, Inc., St. Mary's, OH, USA) and stored at room temperature in the dark. Upon arrival, 16 randomly healthy larvae between ~200 and 250 mg were selected for the experiment. An MRSA MW2 overnight culture was washed with PBS twice and then diluted in PBS to $\sim 1 \times 10^8$ CFU/ml. A 10- μ l inoculum was injected into the rear left proleg of the larvae using a 10- μ l Hamilton syringe (Sigma-Aldrich; catalog no. 24574). Before injection, the syringe was washed with 10% bleach, 70% ethanol, water, and PBS. This washing step was repeated after every six larva injections. After 1 h, 10 μ l PBS containing 20-mg/kg (0.5 mg/ml) PQ401 or 25-mg/kg (0.625 mg/ml) vancomycin was administered into the rear right proleg. The wax moths were incubated at 37°C. Survival was monitored every 24 h for up to 120 h. Statistical analyses (Kaplan-Meier survival analysis and with log rank test) were conducted using GraphPad Prism version 8 (GraphPad Software, La Jolla, CA, USA). A *P* value of less than 0.05 was considered significant.

SUPPLEMENTAL MATERIAL

Supplemental material is available online only.

FIG S1, PDF file, 1.5 MB.

MOVIE S1, MOV file, 2.1 MB.

MOVIE S2, MOV file, 7.1 MB.

MOVIE S3, MOV file, 1.8 MB.

MOVIE S4, MOV file, 0.9 MB.

MOVIE S5, MOV file, 1.8 MB.

MOVIE S6, MOV file, 3 MB.

MOVIE S7, MOV file, 3 MB.

MOVIE S8, MOV file, 3 MB.

MOVIE S9, MOV file, 3 MB.

ACKNOWLEDGMENTS

This study was supported by National Institutes of Health grant P01AI083214 to F.M.A. and E.M. W.K. is supported by the National Research Foundation of Korea grants funded by the South Korean government (MSIT) (2020R1C1C1008842, 2018R1A5A2025286, and 2017M3A9E4077234). G.Z. and H.G. acknowledge support from a start-up grant from the Nanyang Technological University and Institute of High Performance Computing, A*STAR, Singapore. Molecular dynamics simulations reported were performed on resources of the National Supercomputing Centre, Singapore (<http://www.nsc.sg>).

W.K. conducted compound screening. W.K., W.P., S.M.K., R.K., S.L., K.L., and I.E. designed, performed, and analyzed MIC assays, time-kill assays, membrane permeability assays, hemolysis assays, and animal infection assays. W.K., N.F., H.A.F., and P.M.V. designed, performed, and analyzed GUV experiments. G.Z. and H.G. designed, performed, and analyzed MD simulation. W.K., P.M.V., H.G., F.M.A., and E.M. contributed reagents/materials/analysis tools. F.M.A. provided strategic guidance. E.M. supervised the project. W.K., G.Z., H.G., F.M.A., and E.M. wrote the manuscript.

F.M.A. and E.M. have financial interests in Genma Biosciences, Inc., and Octagon Therapeutics, Inc., companies that were previously engaged in developing antimicrobial compounds. E.M.'s and F.M.A.'s interests were reviewed and are managed by Rhode Island Hospital (E.M.) and Massachusetts General Hospital and Partners HealthCare (F.M.A.) in accordance with their conflict of interest policies. The remaining authors declare no competing financial interests.

REFERENCES

1. Tong SYC, Davis JS, Eichenberger E, Holland TL, Fowler VG. 2015. *Staphylococcus aureus* infections: epidemiology, pathophysiology, clinical manifestations, and management. *Clin Microbiol Rev* 28:603–661. <https://doi.org/10.1128/CMR.00134-14>.
2. Haaber J, Penadés JR, Ingmer H. 2017. Transfer of antibiotic resistance in *Staphylococcus aureus*. *Trends Microbiol* 25:893–905. <https://doi.org/10.1016/j.tim.2017.05.011>.
3. Allison KR, Brynildsen MP, Collins JJ. 2011. Metabolite-enabled eradication of bacterial persisters by aminoglycosides. *Nature* 473:216–220. <https://doi.org/10.1038/nature10069>.
4. Conlon BP, Nakayasu ES, Fleck LE, LaFleur MD, Isabella VM, Coleman K, Leonard SN, Smith RD, Adkins JN, Lewis K. 2013. Activated ClpP kills persisters and eradicates a chronic biofilm infection. *Nature* 503:365–370. <https://doi.org/10.1038/nature12790>.
5. Conlon BP, Rowe SE, Gandt AB, Nuxoll AS, Donegan NP, Zalis EA, Clair G, Adkins JN, Cheung AL, Lewis K. 2016. Persister formation in *Staph-*

- Staphylococcus aureus* is associated with ATP depletion. *Nat Microbiol* 1:16051. <https://doi.org/10.1038/nmicrobiol.2016.51>.
6. Kim W, Zou G, Hari TPA, Wilt IK, Zhu W, Galle N, Faizi HA, Hendricks GL, Tori K, Pan W, Huang X, Steele AD, Csatory EE, Dekarske MM, Rosen JL, Ribeiro NDQ, Lee K, Port J, Fuchs BB, Vlahovska PM, Wuest WM, Gao H, Ausubel FM, Mylonakis E. 2019. A selective membrane-targeting repurposed antibiotic with activity against persistent methicillin-resistant *Staphylococcus aureus*. *Proc Natl Acad Sci U S A* 116:16529–16534. <https://doi.org/10.1073/pnas.1904700116>.
 7. Zalis EA, Nuxoll AS, Manuse S, Clair G, Radlinski LC, Conlon BP, Adkins J, Lewis K, Bonomo RA, Michiels J, Mylonakis E. 2019. Stochastic variation in expression of the tricarboxylic acid cycle produces persister cells. *mBio* 10:e01930-19. <https://doi.org/10.1128/mBio.01930-19>.
 8. Keren I, Kaldalu N, Spoering A, Wang Y, Lewis K. 2004. Persister cells and tolerance to antimicrobials. *FEMS Microbiol Lett* 230:13–18. [https://doi.org/10.1016/S0378-1097\(03\)00856-5](https://doi.org/10.1016/S0378-1097(03)00856-5).
 9. Balaban NQ, Helaine S, Lewis K, Ackermann M, Aldridge B, Andersson DI, Brynildsen MP, Bumann D, Camilli A, Collins JJ, Dehio C, Fortune S, Ghigo J-M, Hardt W-D, Harms A, Heinemann M, Hung DT, Jenal U, Levin BR, Michiels J, Storz G, Tan M-W, Tenson T, Van Melderen L, Zinkernagel A. 2019. Definitions and guidelines for research on antibiotic persistence. *Nat Rev Microbiol* 17:441–448. <https://doi.org/10.1038/s41579-019-0196-3>.
 10. Lewis K. 2010. Persister cells. *Annu Rev Microbiol* 64:357–372. <https://doi.org/10.1146/annurev.micro.112408.134306>.
 11. Meylan S, Andrews IW, Collins JJ. 2018. Targeting antibiotic tolerance, pathogen by pathogen. *Cell* 172:1228–1238. <https://doi.org/10.1016/j.cell.2018.01.037>.
 12. Gollan B, Grabe G, Michaux C, Helaine S. 2019. Bacterial persisters and infection: past, present, and progressing. *Annu Rev Microbiol* 73:359–385. <https://doi.org/10.1146/annurev-micro-020518-115650>.
 13. Zhang L-J, Gallo RL. 2016. Antimicrobial peptides. *Curr Biol* 26:R14–R19. <https://doi.org/10.1016/j.cub.2015.11.017>.
 14. Hurdle JG, O'Neill AJ, Chopra I, Lee RE. 2011. Targeting bacterial membrane function: an underexploited mechanism for treating persistent infections. *Nat Rev Microbiol* 9:62–75. <https://doi.org/10.1038/nrmicro2474>.
 15. Ghosh C, Haldar J. 2015. Membrane-active small molecules: designs inspired by antimicrobial peptides. *ChemMedChem* 10:1606–1624. <https://doi.org/10.1002/cmdc.201500299>.
 16. Zhang N, Ma S. 2019. Recent development of membrane-active molecules as antibacterial agents. *Eur J Med Chem* 184:111743. <https://doi.org/10.1016/j.ejmech.2019.111743>.
 17. Andersson DI, Hughes D, Kubicek-Sutherland JZ. 2016. Mechanisms and consequences of bacterial resistance to antimicrobial peptides. *Drug Resist Updat* 26:43–57. <https://doi.org/10.1016/j.drup.2016.04.002>.
 18. Fleitas O, Franco OL. 2016. Induced bacterial cross-resistance toward host antimicrobial peptides: a worrying phenomenon. *Front Microbiol* 7:381. <https://doi.org/10.3389/fmicb.2016.00381>.
 19. Kim W, Conery AL, Rajamuthiah R, Fuchs BB, Ausubel FM, Mylonakis E. 2015. Identification of an antimicrobial agent effective against methicillin-resistant *Staphylococcus aureus* persisters using a fluorescence-based screening strategy. *PLoS One* 10:e0127640. <https://doi.org/10.1371/journal.pone.0127640>.
 20. Kim W, Zhu W, Hendricks GL, Van Tyne D, Steele AD, Keohane CE, Fricke N, Conery AL, Shen S, Pan W, Lee K, Rajamuthiah R, Fuchs BB, Vlahovska PM, Wuest WM, Gilmore MS, Gao H, Ausubel FM, Mylonakis E. 2018. A new class of synthetic retinoid antibiotics effective against bacterial persisters. *Nature* 556:103–107. <https://doi.org/10.1038/nature26157>.
 21. Kim W, Steele AD, Zhu W, Csatory EE, Fricke N, Dekarske MM, Jayamani E, Pan W, Kwon B, Sinitsa IF, Rosen JL, Conery AL, Fuchs BB, Vlahovska PM, Ausubel FM, Gao H, Wuest WM, Mylonakis E. 2018. Discovery and optimization of nTZDpa as an antibiotic effective against bacterial persisters. *ACS Infect Dis* 4:1540–1545. <https://doi.org/10.1021/acscinfecdis.8b00161>.
 22. Garuti L, Roberti M, Bottegoni G, Ferraro M. 2016. Diaryl urea: a privileged structure in anticancer agents. *Curr Med Chem* 23:1528–1548. <https://doi.org/10.2174/0929867323666160411142532>.
 23. Zhang Y, Anderson M, Weisman JL, Lu M, Choy CJ, Boyd VA, Price J, Sigal M, Clark J, Connelly M, Zhu F, Guiguemde WA, Jeffries C, Yang L, Lemoff A, Liou AP, Webb TR, Derisi JL, Guy RK. 2010. Evaluation of diarylureas for activity against *Plasmodium falciparum*. *ACS Med Chem Lett* 1:460–465. <https://doi.org/10.1021/ml100083c>.
 24. Cowan N, Dätwyler P, Ernst B, Wang C, Vennerstrom JL, Spangenberg T, Keiser J. 2015. Activities of N,N'-diarylurea MMV665852 analogs against *Schistosoma mansoni*. *Antimicrob Agents Chemother* 59:1935–1941. <https://doi.org/10.1128/AAC.04463-14>.
 25. Brown JR, North EJ, Hurdle JG, Morisseau C, Scarborough JS, Sun D, Korduláková J, Scherman MS, Jones V, Grzegorzewicz A, Crew RM, Jackson M, McNeil MR, Lee RE. 2011. The structure–activity relationship of urea derivatives as anti-tuberculosis agents. *Bioorg Med Chem* 19:5585–5595. <https://doi.org/10.1016/j.bmc.2011.07.034>.
 26. Le P, Kunold E, Maccis R, Rox K, Jennings MC, Ugur I, Reinecke M, Chaves-Moreno D, Hackl MW, Fetzter C, Mandl FAM, Lehmann J, Korotkov VS, Hacker SM, Kuster B, Antes I, Pieper DH, Rohde M, Wuest WM, Medina E, Sieber SA. 2020. Repurposing human kinase inhibitors to create an antibiotic active against drug-resistant *Staphylococcus aureus*, persisters and biofilms. *Nat Chem* 12:145–158. <https://doi.org/10.1038/s41557-019-0378-7>.
 27. Wilhelm S, Carter C, Lynch M, Lowinger T, Dumas J, Smith RA, Schwartz B, Simantov R, Kelley S. 2006. Discovery and development of sorafenib: a multikinase inhibitor for treating cancer. *Nat Rev Drug Discov* 5:835–844. <https://doi.org/10.1038/nrd2130>.
 28. Gable KL, Maddux BA, Penaranda C, Zavadovskaya M, Campbell MJ, Lobo M, Robinson L, Schow S, Kerner JA, Goldfine ID, Youngren JF. 2006. Diarylureas are small-molecule inhibitors of insulin-like growth factor I receptor signaling and breast cancer cell growth. *Mol Cancer Ther* 5:1079–1086. <https://doi.org/10.1158/1535-7163.MCT-05-0397>.
 29. Moy TI, Ball AR, Anklesaria Z, Casadei G, Lewis K, Ausubel FM. 2006. Identification of novel antimicrobials using a live-animal infection model. *Proc Natl Acad Sci U S A* 103:10414–10419. <https://doi.org/10.1073/pnas.0604055103>.
 30. Kim W, Hendricks GL, Lee K, Mylonakis E. 2017. An update on the use of *C. elegans* for preclinical drug discovery: screening and identifying anti-infective drugs. *Expert Opin Drug Discov* 12:625–633. <https://doi.org/10.1080/17460441.2017.1319358>.
 31. Peterson ND, Pukkila-Worley R. 2018. *Caenorhabditis elegans* in high-throughput screens for anti-infective compounds. *Curr Opin Immunol* 54:59–65. <https://doi.org/10.1016/j.coi.2018.06.003>.
 32. Weigel LM, Clewell DB, Gill SR, Clark NC, McDougal LK, Flannagan SE, Kolonay JF, Shetty J, Killgore GE, Tenover FC. 2003. Genetic analysis of a high-level vancomycin-resistant isolate of *Staphylococcus aureus*. *Science* 302:1569–1571. <https://doi.org/10.1126/science.1090956>.
 33. Rice LB. 2008. Federal funding for the study of antimicrobial resistance in nosocomial pathogens: no ESKAPE. *J Infect Dis* 197:1079–1081. <https://doi.org/10.1086/533452>.
 34. García-Solache M, Rice LB. 2016. Genome sequence of the multiantibiotic-resistant *Enterococcus faecium* strain C68 and insights on the pLRM23 colonization plasmid. *Genome Announc* 4:e01719-15. <https://doi.org/10.1128/genomeA.01719-15>.
 35. Foster TJ. 2017. Antibiotic resistance in *Staphylococcus aureus*. *Current status and future prospects*. *FEMS Microbiol Rev* 41:430–449. <https://doi.org/10.1093/femsre/fux007>.
 36. Friedman L, Alder JD, Silverman JA. 2006. Genetic changes that correlate with reduced susceptibility to daptomycin in *Staphylococcus aureus*. *Antimicrob Agents Chemother* 50:2137–2145. <https://doi.org/10.1128/AAC.00039-06>.
 37. Van Bambeke F, Mingeot-Leclercq MP, Struelens MJ, Tulkens PM. 2008. The bacterial envelope as a target for novel anti-MRSA antibiotics. *Trends Pharmacol Sci* 29:124–134. <https://doi.org/10.1016/j.tips.2007.12.004>.
 38. Chen Y-F, Sun T-L, Sun Y, Huang HW. 2014. Interaction of daptomycin with lipid bilayers: a lipid extracting effect. *Biochemistry* 53:5384–5392. <https://doi.org/10.1021/bi500779g>.
 39. Faizi HA, Frey SL, Steinkühler J, Dimova R, Vlahovska PM. 2019. Bending rigidity of charged lipid bilayer membranes. *Soft Matter* 15:6006–6013. <https://doi.org/10.1039/c9sm00772e>.
 40. Dimova R, Aranda S, Bezlyepkina N, Nikolov V, Riske KA, Lipowsky R. 2006. A practical guide to giant vesicles. Probing the membrane nanoregime via optical microscopy. *J Phys Condens Matter* 18:S1151–S1176. <https://doi.org/10.1088/0953-8984/18/28/S04>.
 41. Sudbrack TP, Archilha NL, Itri R, Riske KA. 2011. Observing the solubilization of lipid bilayers by detergents with optical microscopy of GUVs. *J Phys Chem B* 115:269–277. <https://doi.org/10.1021/jp108653e>.
 42. Tamba Y, Yamazaki M. 2005. Single giant unilamellar vesicle method reveals effect of antimicrobial peptide magainin 2 on membrane permeability. *Biochemistry* 44:15823–15833. <https://doi.org/10.1021/bi051684w>.
 43. Ambroggio EE, Separovic F, Bowie JH, Fidelio GD, Bagatolli LA. 2005. Direct visualization of membrane leakage induced by the antibiotic

- peptides: maculatin, citropin, and aurein. *Biophys J* 89:1874–1881. <https://doi.org/10.1529/biophysj.105.066589>.
44. Lee C-C, Sun Y, Qian S, Huang HW. 2011. Transmembrane pores formed by human antimicrobial peptide LL-37. *Biophys J* 100:1688–1696. <https://doi.org/10.1016/j.bpj.2011.02.018>.
 45. Wang Y, Corbitt TS, Jett SD, Tang Y, Schanze KS, Chi EY, Whitten DG. 2012. Direct visualization of bactericidal action of cationic conjugated polyelectrolytes and oligomers. *Langmuir* 28:65–70. <https://doi.org/10.1021/la2044569>.
 46. Lee M-T, Sun T-L, Hung W-C, Huang HW. 2013. Process of inducing pores in membranes by melittin. *Proc Natl Acad Sci U S A* 110:14243–14248. <https://doi.org/10.1073/pnas.1307010110>.
 47. Ganewatta MS, Chen YP, Wang J, Zhou J, Ebalunode J, Nagarkatti M, Decho AW, Tang C. 2014. Bio-inspired resin acid-derived materials as anti-bacterial resistance agents with unexpected activities. *Chem Sci* 5:2011–2016. <https://doi.org/10.1039/c4sc00034j>.
 48. Joshi S, Dewangan RP, Yar MS, Rawat DS, Pasha S. 2015. N-terminal aromatic tag induced self assembly of tryptophan-arginine rich ultra short sequences and their potent antibacterial activity. *RSC Adv* 5:68610–68620. <https://doi.org/10.1039/C5RA12095K>.
 49. Kim W, Fricke N, Conery AL, Fuchs BB, Rajamuthiah R, Jayamani E, Vlahovska PM, Ausubel FM, Mylonakis E. 2016. NH125 kills methicillin-resistant *Staphylococcus aureus* persists by lipid bilayer disruption. *Future Med Chem* 8:257–269. <https://doi.org/10.4155/fmc.15.189>.
 50. Hong C, Tieleman DP, Wang Y. 2014. Microsecond molecular dynamics simulations of lipid mixing. *Langmuir* 30:11993–12001. <https://doi.org/10.1021/la502363b>.
 51. Deleu M, Crowet J-M, Nasir MN, Lins L. 2014. Complementary biophysical tools to investigate lipid specificity in the interaction between bioactive molecules and the plasma membrane: a review. *Biochim Biophys Acta* 1838:3171–3190. <https://doi.org/10.1016/j.bbmem.2014.08.023>.
 52. Zhou X, Zhao X, Li X, Ping G, Pei S, Chen M, Wang Z, Zhou W, Jin B. 2016. PQ401, an IGF-1R inhibitor, induces apoptosis and inhibits growth, proliferation and migration of glioma cells. *J Chemother* 28:44–49. <https://doi.org/10.1179/1973947815Y.0000000026>.
 53. Schmid N, Eichenberger AP, Choutko A, Riniker S, Winger M, Mark AE, van Gunsteren WF. 2011. Definition and testing of the GROMOS force-field versions 54A7 and 54B7. *Eur Biophys J* 40:843–856. <https://doi.org/10.1007/s00249-011-0700-9>.
 54. Malde AK, Zuo L, Breeze M, Stroet M, Poger D, Nair PC, Oostenbrink C, Mark AE. 2011. An automated force field topology builder (ATB) and repository: version 1.0. *J Chem Theory Comput* 7:4026–4037. <https://doi.org/10.1021/ct200196m>.
 55. Stroet M, Caron B, Visscher KM, Geerke DP, Malde AK, Mark AE. 2018. Automated topology builder version 3.0: prediction of solvation free enthalpies in water and hexane. *J Chem Theory Comput* 14:5834–5845. <https://doi.org/10.1021/acs.jctc.8b00768>.
 56. Hub JS, de Groot BL, van der Spoel D. 2010. g_wham—a free weighted histogram analysis implementation including robust error and autocorrelation estimates. *J Chem Theory Comput* 6:3713–3720. <https://doi.org/10.1021/ct100494z>.
 57. Sakagami Y, Iinuma M, Piyasena K, Dharmaratne H. 2005. Antibacterial activity of alpha-mangostin against vancomycin resistant enterococci (VRE) and synergism with antibiotics. *Phytomedicine* 12:203–208. <https://doi.org/10.1016/j.phymed.2003.09.012>.
 58. Cutuli MA, Petronio Petronio G, Veralgato F, Magnifico I, Pietrangelo L, Venditti N, Di Marco R. 2019. *Galleria mellonella* as a consolidated *in vivo* model hosts: new developments in antibacterial strategies and novel drug testing. *Virulence* 10:527–541. <https://doi.org/10.1080/21505594.2019.1621649>.
 59. Mingeot-Leclercq MP, Décout J-L. 2016. Bacterial lipid membranes as promising targets to fight antimicrobial resistance, molecular foundations and illustration through the renewal of aminoglycoside antibiotics and emergence of amphiphilic aminoglycosides. *Med Chem Commun (Camb)* 7:586–611. <https://doi.org/10.1039/C5MD00503E>.
 60. Hodille E, Rose W, Diep BA, Goutelle S, Lina G, Dumitrescu O. 2017. The role of antibiotics in modulating virulence in *Staphylococcus aureus*. *Clin Microbiol Rev* 30:887–917. <https://doi.org/10.1128/CMR.00120-16>.
 61. Liu Q, Zheng Z, Kim W, Fuchs BB, Mylonakis E. 2018. Influence of subinhibitory concentrations of NH125 on biofilm formation & virulence factors of *Staphylococcus aureus*. *Future Med Chem* 10:1319–1331. <https://doi.org/10.4155/fmc-2017-0286>.
 62. Greenfield BK, Shaked S, Marrs CF, Nelson P, Raxter I, Xi C, McKone TE, Jolliet O. 2017. Modeling the emergence of antibiotic resistance in the environment: an analytical solution for the minimum selection concentration. *Antimicrob Agents Chemother* 62:e01686-17. <https://doi.org/10.1128/AAC.01686-17>.
 63. Marcos JF, Muñoz A, Pérez-Payá E, Misra S, López-García B. 2008. Identification and rational design of novel antimicrobial peptides for plant protection. *Annu Rev Phytopathol* 46:273–301. <https://doi.org/10.1146/annurev.phyto.121307.094843>.
 64. Mylonakis E, Podsiadlowski L, Muhammed M, Vilcinskas A. 2016. Diversity, evolution and medical applications of insect antimicrobial peptides. *Philos Trans R Soc B* 371:20150290. <https://doi.org/10.1098/rstb.2015.0290>.
 65. Omardien S, Brul S, Zaat S. 2016. Antimicrobial activity of cationic antimicrobial peptides against Gram-positives: current progress made in understanding the mode of action and the response of bacteria. *Front Cell Dev Biol* 4:111. <https://doi.org/10.3389/fcell.2016.00111>.
 66. Mishra B, Reiling S, Zarena D, Wang G. 2017. Host defense antimicrobial peptides as antibiotics: design and application strategies. *Curr Opin Chem Biol* 38:87–96. <https://doi.org/10.1016/j.cbpa.2017.03.014>.
 67. Miller WR, Bayer AS, Arias CA. 2016. Mechanism of action and resistance to daptomycin in *Staphylococcus aureus* and *Enterococci*. *Cold Spring Harb Perspect Med* 6:a026997. <https://doi.org/10.1101/cshperspect.a026997>.
 68. Bayer AS, Mishra NN, Sakoulas G, Nonejuie P, Nast CC, Pogliano J, Chen K-T, Ellissen SN, Yeaman MR, Yang S-J. 2014. Heterogeneity of *mprF* sequences in methicillin-resistant *Staphylococcus aureus* clinical isolates: role in cross-resistance between daptomycin and host defense antimicrobial peptides. *Antimicrob Agents Chemother* 58:7462–7467. <https://doi.org/10.1128/AAC.03422-14>.
 69. Mishra NN, Bayer AS, Weidenmaier C, Grau T, Wanner S, Stefani S, Cafiso V, Bertuccio T, Yeaman MR, Nast CC, Yang S-J. 2014. Phenotypic and genotypic characterization of daptomycin-resistant methicillin-resistant *Staphylococcus aureus* strains: relative roles of *mprF* and *dlt* operons. *PLoS One* 9:e107426. <https://doi.org/10.1371/journal.pone.0107426>.
 70. Sezer D, Oruç T. 2017. Protonation kinetics compromise liposomal fluorescence assay of membrane permeation. *J Phys Chem B* 121:5218–5227. <https://doi.org/10.1021/acs.jpcc.7b01881>.
 71. Doktorova M, Harries D, Khelashvili G. 2017. Determination of bending rigidity and tilt modulus of lipid membranes from real-space fluctuation analysis of molecular dynamics simulations. *Phys Chem Chem Phys* 19:16806–16818. <https://doi.org/10.1039/c7cp01921a>.
 72. Osher E, Macaulay VM. 2019. Therapeutic targeting of the IGF axis. *Cells* 8:895. <https://doi.org/10.3390/cells8080895>.
 73. Pautsch A, Zoepfel A, Ahorn H, Spevak W, Hauptmann R, Nar H. 2001. Crystal structure of bisphosphorylated IGF-1 receptor kinase: insight into domain movements upon kinase activation. *Structure* 9:955–965. [https://doi.org/10.1016/s0969-2126\(01\)00655-4](https://doi.org/10.1016/s0969-2126(01)00655-4).
 74. Steiner L, Blum G, Friedmann Y, Levitzki A. 2007. ATP non-competitive IGF-1 receptor kinase inhibitors as lead anti-neoplastic and anti-papilloma agents. *Eur J Pharmacol* 562:1–11. <https://doi.org/10.1016/j.ejphar.2007.01.052>.
 75. Yang Y, Shen J, Yu X, Qin G, Zhang M, Shen H, Mao Z, Ferrari M. 2013. Identification of an inhibitory mechanism of luteolin on the insulin-like growth factor-1 ligand-receptor interaction. *Chembiochem* 14:929–933. <https://doi.org/10.1002/cbic.201300082>.
 76. Moriev R, Vasylychenko O, Platonov M, Grygorenko O, Volkova K, Zozulya S. 2013. Identification of novel IGF1R kinase inhibitors by molecular modeling and high-throughput screening. *Acta Naturae* 5:90–99. <https://doi.org/10.32607/20758251-2013-5-2-90-99>.
 77. Jin Q, Nie H, McClelland BW, Widdowson KL, Palovich MR, Elliott JD, Goodman RM, Burman M, Sarau HM, Ward KW, Nord M, Orr BM, Gorycki PD, Busch-Petersen J. 2004. Discovery of potent and orally bioavailable N,N'-diaryllurea antagonists for the CXCR2 chemokine receptor. *Bioorg Med Chem Lett* 14:4375–4378. <https://doi.org/10.1016/j.bmcl.2004.06.097>.
 78. Zarghi A, Kakhgi S, Hadipoor A, Daraee B, Dadrass OG, Hedayati M. 2008. Design and synthesis of 1,3-diaryllurea derivatives as selective cyclooxygenase (COX-2) inhibitors. *Bioorg Med Chem Lett* 18:1336–1339. <https://doi.org/10.1016/j.bmcl.2008.01.021>.
 79. Wu J, Wang C, Leas D, Vargas M, White KL, Shackelford DM, Chen G, Sanford AG, Hemsley RM, Davis PH, Dong Y, Charman SA, Keiser J, Vennerstrom JL. 2018. Progress in antischistosomal N,N'-diaryl urea

- SAR. *Bioorg Med Chem Lett* 28:244–248. <https://doi.org/10.1016/j.bmcl.2017.12.064>.
80. Baba T, Bae T, Schneewind O, Takeuchi F, Hiramatsu K. 2008. Genome sequence of *Staphylococcus aureus* strain Newman and comparative analysis of Staphylococcal genomes: polymorphism and evolution of two major pathogenicity islands. *J Bacteriol* 190:300–310. <https://doi.org/10.1128/JB.01000-07>.
 81. Baba T, Takeuchi F, Kuroda M, Yuzawa H, Aoki K-I, Oguchi A, Nagai Y, Iwama N, Asano K, Naimi T, Kuroda H, Cui L, Yamamoto K, Hiramatsu K. 2002. Genome and virulence determinants of high virulence community-acquired MRSA. *Lancet* 359:1819–1827. [https://doi.org/10.1016/S0140-6736\(02\)08713-5](https://doi.org/10.1016/S0140-6736(02)08713-5).
 82. Fey PD, Endres JL, Yajjala VK, Widhelm TJ, Boissy RJ, Bose JL, Bayles KW. 2013. A genetic resource for rapid and comprehensive phenotype screening of nonessential *Staphylococcus aureus* genes. *mBio* 4:e00537-12. <https://doi.org/10.1128/mBio.00537-12>.
 83. Garsin DA, Sifri CD, Mylonakis E, Qin X, Singh KV, Murray BE, Calderwood SB, Ausubel FM. 2001. A simple model host for identifying Gram-positive virulence factors. *Proc Natl Acad Sci U S A* 98:10892–10897. <https://doi.org/10.1073/pnas.191378698>.
 84. Rice LB, Carias LL, Rudin S, Lakticová V, Wood A, Hutton-Thomas R. 2005. *Enterococcus faecium* low-affinity pbp5 is a transferable determinant. *Antimicrob Agents Chemother* 49:5007–5012. <https://doi.org/10.1128/AAC.49.12.5007-5012.2005>.
 85. Carias LL, Rudin SD, Donskey CJ, Rice LB. 1998. Genetic linkage and cotransfer of a novel, *vanB*-containing transposon (Tn5382) and a low-affinity penicillin-binding protein 5 gene in a clinical vancomycin-resistant *Enterococcus faecium* isolate. *J Bacteriol* 180:4426–4434. <https://doi.org/10.1128/JB.180.17.4426-4434.1998>.
 86. Smith MG, Gianoulis TA, Pukatzki S, Mekalanos JJ, Ornston LN, Gerstein M, Snyder M. 2007. New insights into *Acinetobacter baumannii* pathogenesis revealed by high-density pyrosequencing and transposon mutagenesis. *Genes Dev* 21:601–614. <https://doi.org/10.1101/gad.1510307>.
 87. Rahme LG, Stevens EJ, Wolfort SF, Shao J, Tompkins RG, Ausubel FM. 1995. Common virulence factors for bacterial pathogenicity in plants and animals. *Science* 268:1899–1902. <https://doi.org/10.1126/science.7604262>.
 88. Clinical and Laboratory Standards Institute. 2012. Methods for dilution antimicrobial susceptibility tests for bacteria that grow aerobically; approved standard-9th ed. CLSI document M07-A9. Clinical and Laboratory Standards Institute, Wayne, PA.
 89. Pankey GA, Sabath LD. 2004. Clinical relevance of bacteriostatic versus bactericidal mechanisms of action in the treatment of Gram-positive bacterial infections. *Clin Infect Dis* 38:864–870. <https://doi.org/10.1086/381972>.
 90. Hess B, Kutzner C, van der Spoel D, Lindahl E. 2008. GROMACS 4: algorithms for highly efficient, load-balanced, and scalable molecular simulation. *J Chem Theory Comput* 4:435–447. <https://doi.org/10.1021/ct700301q>.
 91. Berger O, Edholm O, Jähnig F. 1997. Molecular dynamics simulations of a fluid bilayer of dipalmitoylphosphatidylcholine at full hydration, constant pressure, and constant temperature. *Biophys J* 72:2002–2013. [https://doi.org/10.1016/S0006-3495\(97\)78845-3](https://doi.org/10.1016/S0006-3495(97)78845-3).
 92. Berendsen HJC, Grigera JR, Straatsma TP. 1987. The missing term in effective pair potentials. *J Phys Chem* 91:6269–6271. <https://doi.org/10.1021/j100308a038>.
 93. Tu Y, Lv M, Xiu P, Huynh T, Zhang M, Castelli M, Liu Z, Huang Q, Fan C, Fang H, Zhou R. 2013. Destructive extraction of phospholipids from *Escherichia coli* membranes by graphene nanosheets. *Nat Nanotechnol* 8:594–601. <https://doi.org/10.1038/nnano.2013.125>.
 94. Zhu W, Bussche von Dem A, Yi X, Qiu Y, Wang Z, Weston P, Hurt RH, Kane AB, Gao H. 2016. Nanomechanical mechanism for lipid bilayer damage induced by carbon nanotubes confined in intracellular vesicles. *Proc Natl Acad Sci U S A* 113:12374–12379. <https://doi.org/10.1073/pnas.1605030113>.
 95. Essmann U, Perera L, Berkowitz ML, Darden T, Lee H, Pedersen LG. 1995. A smooth particle mesh Ewald method. *J Chem Phys* 103:8577–8593. <https://doi.org/10.1063/1.470117>.
 96. Creighton MA, Zhu W, van Krieken F, Petteruti RA, Gao H, Hurt RH. 2016. Three-dimensional graphene-based microbarriers for controlling release and reactivity in colloidal liquid phases. *ACS Nano* 10:2268–2276. <https://doi.org/10.1021/acsnano.5b06963>.
 97. Isralewitz B, Gao M, Schulten K. 2001. Steered molecular dynamics and mechanical functions of proteins. *Curr Opin Struct Biol* 11:224–230. [https://doi.org/10.1016/S0959-440x\(00\)00194-9](https://doi.org/10.1016/S0959-440x(00)00194-9).
 98. Kumar S, Rosenberg JM, Bouzida D, Swendsen RH, Kollman PA. 1992. The weighted histogram analysis method for free-energy calculations on biomolecules. I. The method. *J Comput Chem* 13:1011–1021. <https://doi.org/10.1002/jcc.540130812>.
 99. Rajamuthiah R, Fuchs BB, Jayamani E, Kim Y, Larkins-Ford J, Conery A, Ausubel FM, Mylonakis E. 2014. Whole animal automated platform for drug discovery against multi-drug resistant *Staphylococcus aureus*. *PLoS One* 9:e89189. <https://doi.org/10.1371/journal.pone.0089189>.
 100. Beanan MJ, Strome S. 1992. Characterization of a germ-line proliferation mutation in *C. elegans*. *Development* 116:755–766.
 101. Anastassopoulou CG, Fuchs BB, Mylonakis E. 2011. *Caenorhabditis elegans*-based model systems for antifungal drug discovery. *Curr Pharm Des* 17:1225–1233. <https://doi.org/10.2174/138161211795703753>.
 102. Hino MT, Sagasti A, Hisamoto N, Kawasaki M, Nakano S, Tsuji JN, Bargmann CI, Matsumoto K. 2002. SEK-1 MAPKK mediates Ca²⁺ signaling to determine neuronal asymmetric development in *Caenorhabditis elegans*. *EMBO Rep* 3:56–62. <https://doi.org/10.1093/embo-reports/kvf001>.
 103. Tan MW, Mahajan-Miklos S, Ausubel FM. 1999. Killing of *Caenorhabditis elegans* by *Pseudomonas aeruginosa* used to model mammalian bacterial pathogenesis. *Proc Natl Acad Sci U S A* 96:715–720. <https://doi.org/10.1073/pnas.96.2.715>.